European Polymer Journal 143 (2021) 110188

Contents lists available at ScienceDirect

European Polymer Journal

journal homepage: www.elsevier.com/locate/europolj

Biomimetic adhesion motifs based on RAFT polymers with phosphonate groups

Patrick Steinbauer [a,b,e], Andreas Rohatschek [c,e,f], Orestis Andriotis [c,e], Nikolaos Bouropoulos [d,g], Robert Liska [b,e,f], Philipp J. Thurner [c,e,f,*,1], Stefan Baudis [a,b,e,f,*,1]

[a] Christian Doppler Laboratory for Advanced Polymers for Biomaterials and 3D Printing, TU Wien, 1060 Vienna, Austria
[b] Institute of Applied Synthetic Chemistry, Division of Macromolecular Chemistry, TU Wien, 1060 Vienna, Austria
[c] Institute of Lightweight Design and Structural Biomechanics, TU Wien, 1060 Vienna, Austria
[d] Department of Materials Science, University of Patras, GR-26504 Rio Patras, Greece
[e] Austrian Cluster for Tissue Regeneration, 1200 Vienna, Austria
[f] Biointerface Doctorate School, TU Wien, 1060 Vienna, Austria
[g] Foundation for Research and Technology Hellas, Institute of Chemical Engineering and High Temperature Chemical Processes, FORTH/ICE-HT, 26504 Patras, Greece

ARTICLE INFO

Keywords:
RAFT polymerization
Atomic Force Microscopy (AFM)
Single-Molecule Force Spectroscopy (SMFS)
Biomimetic Adhesion Motif
Adhesion Measurement

ABSTRACT

Adhesion processes play a decisive role in the animal and human body and have been studied in great detail. Phosphorylation of serine as adhesion strategy is found in different species and serves different purposes, e.g. under water surface adhesion and protection strategies. Based on these biological adhesion applications, we present a biomimetic phosphonate-containing block copolymer approach to study surface adhesion. We synthesized two block copolymers (28 kDa and 39 kDa), which differed in their phosphonate-containing block dimethyl(2-methacryloyloxyethyl phosphonate) (DMMEP), using reversible addition fragmentation-chain transfer (RAFT) polymerization and tethered these polymers onto atomic force microscopy (AFM) probes. After performing AFM in single molecule force spectroscopy (SMFS) mode under physiological-like conditions (phosphate buffered saline - PBS, pH 7.2) on different substrates (mica, calcium deficient hydroxyapatite, TiO_2 coated Si-wafer) we determined adhesion forces of 1610 ± 76 pN and 2257 ± 48 pN for the 28 kDa and the 39 kDa block copolymer, respectively. Our results show higher adhesion on hydroxyapatite, TiO_2 and mica using polymers with a longer phosphonate block. This phosphonate containing block copolymer could serve as adhesion motif in several applications, and is very promising in the biomedical field, especially for tissue engineering applications due to its excellent adhesion on hydroxyapatite and titanium under physiological-like conditions.

1. Introduction

Adhesion is crucial in many biological processes. Thus, bioinspired adhesion strategies as a basis of novel adhesion technologies have been the subject of a number of studies, especially in biomedical engineering. [1]

In this context and based on the adhesion mechanism identified, phosphorylation of serine is an occurring modification for adhesion in several species.[1] In the blue mussel (*Mytilus edulis),* foot protein 5 (Mfp-5) contains L-3,4-dihydroxyphenylalanine (DOPA), lysines, glycines and phosphoserines, which promote the mussel adhesion on various surfaces under wet and salty environment.[2,3] Phosphoserines and lysine-rich proteins are prominent in protein Pc-3, which is responsible for complex coacervation in the sandcastle worm (*Phragmatopoma californica)* (Fig. 1a).[4,5] High content of phosphoserine in proteines are used by caddisfly larvae to glue grains of sand for protective defense (Fig. 1a).[6–8] These phosphoserines also participate in the adhesion of sea stars.[9] In the bone and tooth matrix phosphoserine-rich proteins, the so called non-collagenous proteins (NCPs), play a decisive role on both bone ultrastructure and bone fracture mechanics (Fig. 1b). NCPs influence bone mineralization by controlling hydroxyapatite crystal size and shape,[10] the formation of collagen fibrils and cell matrix interactions. Thus, modifications of NCPs can affect the mechanical properties[11–13] of bone. Before the insight

* Corresponding authors at: Getreidemarkt 9/E163, 1060 Vienna, Austria (S. Baudis). Getreidemarkt 9/E317, 1060 Vienna, Austria (P.J. Thurner).
E-mail addresses: philipp.thurner@tuwien.ac.at (P.J. Thurner), stefan.baudis@tuwien.ac.at (S. Baudis).
[1] Authors contributed equally to this manuscript.

https://doi.org/10.1016/j.eurpolymj.2020.110188
Received 30 September 2020; Received in revised form 23 November 2020; Accepted 29 November 2020
Available online 7 December 2020

on NCPs role, bisphosphonates were used in osteoporosis treatment (Fig. 1c).[14–16] Commercially available osteoporotic drugs consist of bisphosphonates, which have a P-C-P bond that is highly resistant to chemical and enzymatic hydrolysis. These molecules have a high affinity to hydroxyapatite in bone and inhibit bone resorption by inhibition of osteoclast function.[17] Bisphosphonates as bone targeting ligands are also attractive for the treatment of Pagets disease and bone metastatic cancer.[18]

Additionally, possible use of biomimetic polymers may be also found for tissue engineering applications. For example, Long *et al.*[19] stated that a six amino acid long N-terminus motif of the salivary protein statherin (DpSpSEEK) is responsible for adhesion on hydroxyapatite (HAP). In a previous study we could corroborate this significant adhesion of the motif by comparing the naturally occurring phosphorylated motif with an unphosphorylated variant (DSSEKC) on calcium deficient hydroxyapatite (CDHAP) and on a TiO_2 coated silicon wafer.[20] This dependence of adhesion on phosphorylation suggests a potential adhesion-by-demand mechanism in biological systems driven by up- or down-regulated phosphorylation.

The applicability in the biomedical field is very promising due to strong interactions with dentin, enamel or bone as well as implants. Strong adhesion occurs caused by covalent, ionic bonds and complex formation with calcium ions on the tooth surface or with titanium ions on the implant surface.[21] So-called, primer molecules consisting of phosphonic acid or phosphonate groups are frequently used in the dental industry (Fig. 1d). These primer molecules are composed of an adhesion motif (AM), a spacer and one or more polymerizable groups (PG). The adhesion motif is creating a bond between dentin and enamel. The spacer is responsible for hydrophilicity, swelling properties, flexibility and stiffness.[21] For the free-radical polymerizable groups, methacrylates have proven to be very efficient and reactive. A widely used dental primer for better adhesion of the restorative is 10-methacryloyloxydecyl dihydrogen phosphate (MDP) (Fig. 1c).[21]

Research and characterization of biomimetic phosphonate-based polymers for various applications started already several years ago [22,23] and is now massively increasing.[24] Further investigations in the animal kingdom and the human body are revealing the great potential of different proteins with phosphonate groups.[3] Such materials are used industrially for binding to metals due to their complexing properties[25–28] as well as dispersants,[29] flame-retardants[30,31] and corrosion inhibiting agents.[32] Preparation of many phosphorus-based polymers has been realized by free radical polymerization, especially photopolymerization. Several research groups dealt with living radical polymerization like Reversible Addition Fragmentation-chain Transfer (RAFT) polymerization[33–35] for synthesis of adhesive polymers.[36–39] This polymerization technique allows synthesis of well-defined polymers with different architectures (e.g. block copolymers,[40–42] graft and comb polymers,[43,44] star polymers, [45–47] hyper branched[48,49] and dendritic polymers[50,51]) under various reaction conditions.

In this study, biomimetic block copolymers with a neutral functional group, serving as an anchorage point for further modifications, and an adhesive block, allowing adhesion to hydroxyapatite and titanium surfaces, were synthesized. The neutral moiety consists of 2-hydroxyethyl methacrylate (HEMA) and the adhesive part of dimethyl (2-methacryloyloxyethyl phosphonate) (DMMEP). In the latter, the block length was varied to generate a different number of adhesion points. Thus, the block copolymers can be analyzed according their pull-off force and the effects of the longer DMMEP block can be investigated. Therefore, AFM tips were functionalized with biomimetic block copolymers and characterized using atomic force microscopy (AFM) in the single force spectroscopy mode under physiological conditions (PBS, pH 7.2) on different substrates (mica, CDHAP, TiO_2 coated silicon wafer).

2. Results and discussion

2.1. Adhesive block copolymers and synthesis thereof

2.1.1. Synthesis of monomer and RAFT agent

To mimic phosphorylated serines in adhesive peptide sequences, dimethyl (2-methacryloyl-oxyethyl phosphonate) DMMEP was chosen, containing a phosphonate group. The synthesis of DMMEP was based on

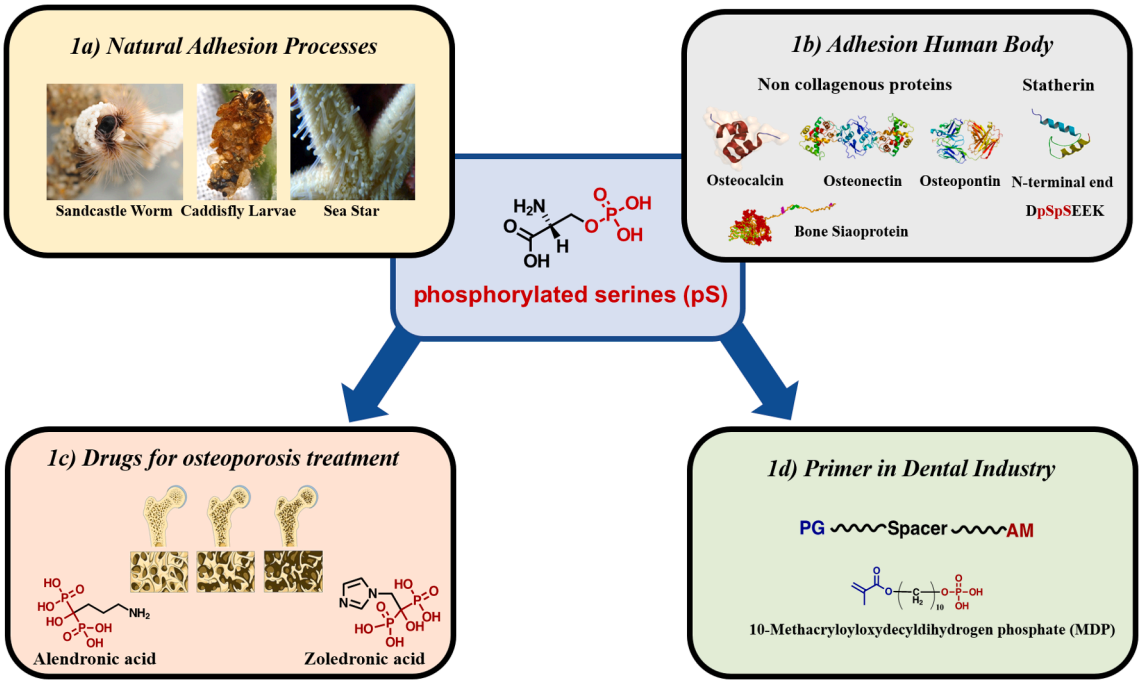

Fig. 1. Natural occurring adhesion and bioinspired adhesion applications. a) Natural adhesion processes based on phosphoserines in sandcastle worm, caddisfly larvae and sea stars. b) Adhesion processes in the human body via non-collagenous proteins (osteocalcin, osteonectin, osteopontin, bone sialoprotein, etc.) and the salivary protein statherin. c) Bisphosphonates as drugs for treatment of osteoporosis. d) Primer molecules in dental industry consisting of an adhesion motif (AM), spacer and a polymerizable group (PG).

the procedure according to Avci and Albayrak.[52] 1 eq. of dimethyl (2-hydroxyethyl) phosphonate was reacted with an excess of methacryloyl chloride in the presence of triethylamine (TEA) under Schotten-Baumann conditions (Fig. 2). After the work-up procedure evaporation of solvent gave the product as yellow, viscous liquid in a yield of 75% and 98% purity.

The synthesis of the RAFT agent 2-cyanoprop-2-yldithiobenzoate (CPDB) was performed in a three-step procedure. First, the synthesis of sodium dithiobenzoate (DTBA), was carried out in accordance to Mitsukami's[53] modification of the method published by Becke and Hagen.[54] 1 eq. of benzyl chloride, 2 eq. of sodium methoxide (30% solution in methanol) and 2 eq. of elemental sulfur were reacted. After purification, the product was obtained as a solution of sodium dithiobenzoate in deionized water. Second, DTBA was oxidized via potassium ferricyanide (III) to di(thiobenzoyl) disulfide (DTBDS) according to Mitsukami *et al.*[53] To circumvent decomposition of the red solid product, DTBDS was directly used for the next step without any purification step. Third, the synthesis of 2-cyanoprop-2-yldithiobenzoate (CPDB) was carried out according to Thang *et al.*[55] DTBDS was added to 2,2′–azobis(isobutyronitrile) (AIBN) under argon atmosphere. The crude product was purified via column chromatography to give CPDB in a yield of 52% as red viscous liquid.

2.1.2. Synthesis of adhesive block copolymers via RAFT polymerization

To synthesize biomimetic adhesive block copolymers for possible medical applications, RAFT polymerization was used for controlling polymerization of monomers. Two different block copolymers with different length of the adhesive block were synthesized using CPDB and the monomers HEMA and DMMEP (Fig. 2). The last step was the end group removal of the thiocarbonylthio group to generate a thiol functionality for adhesion measurement via AFM based SMFS.

The homopolymerization of HEMA was carried out in accordance to Vega–Rios.[56] First, the monomer (concentration 1.5 mol L^{-1}), CPDB, the initiator (AIBN) and the internal standard (naphthalene) were mixed. A theoretical molecular weight of 14 kDa for the HEMA homopolymer was calculated using Equation 1 (Supporting Information S6). The structure and molecular weight of the homopolymer (pHEMA) was confirmed using ^{1}H NMR and GPC analysis. The polymerization kinetics were monitored by drawing samples over the whole course of reaction. The most efficient CTA to initiator ratio for pHEMA was 1:0.02 (see Table 1). The conversion was determined via the percental decrease of the methacrylate integrals with respect to the internal standard (see Supporting Information S6 Equation 2). RAFT polymerization of HEMA is different to well-known RAFT-polymerizations like methylmethacrylate (MMA). Although both monomers are methacrylates, they have a quite different polymerization behavior and different solvation (HEMA is hydrophilic, MMA hydrophobic).[56] It is necessary to increase the CTA to initiator ratio to values between 25 and 50 for controlling the molecular weight and polydispersity, due to the low transfer ability of HEMA to the CTA.[56] The controlled radical polymerization of HEMA was only possible at low monomer conversion (<30%) as also reported in literature.[56] In this region, however, the polymerization proceeds well-controlled following a linear course of $M_{n,NMR}$ (molecular weight determined via NMR), whereby the molar mass dispersity (Đ)

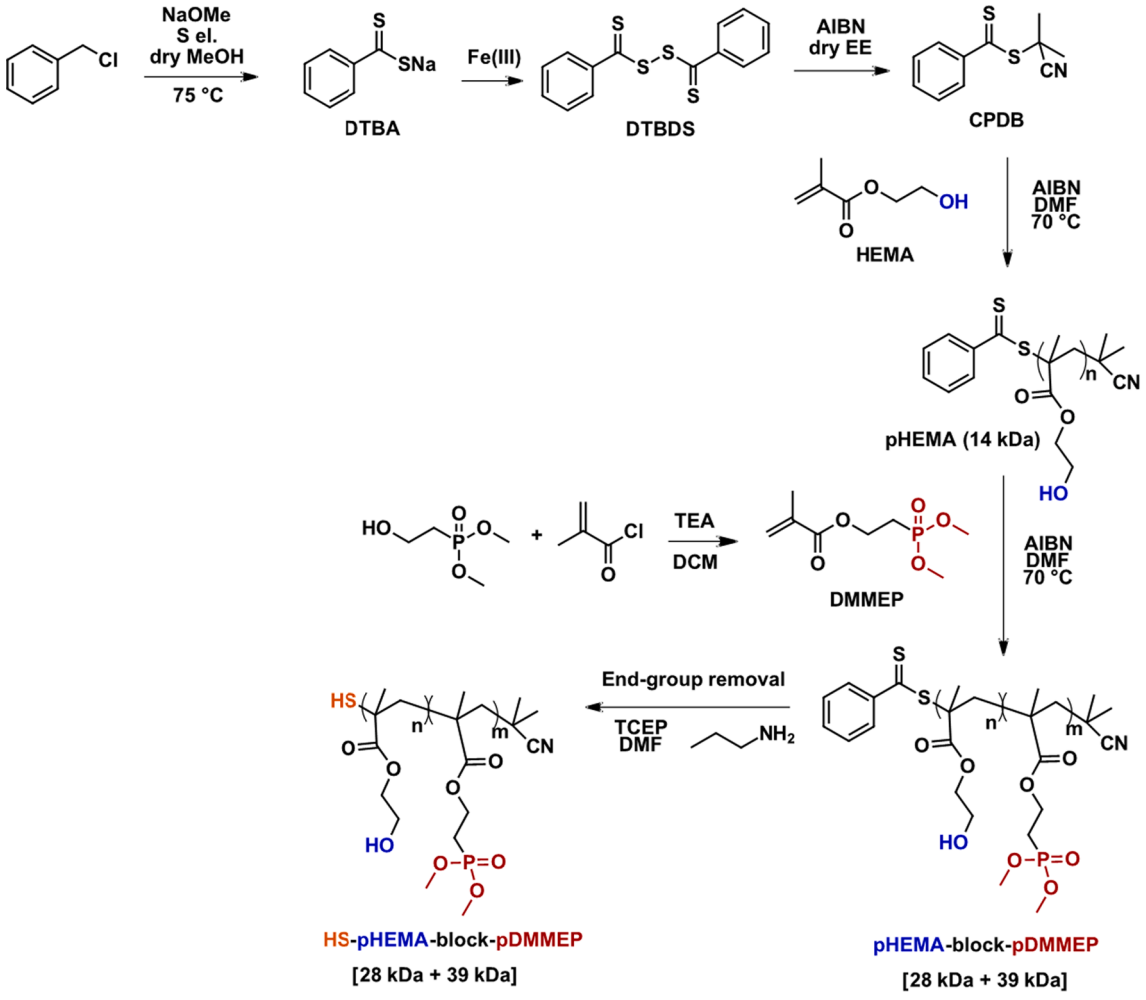

Fig. 2. Preparation of HS-pHEMA-block-pDMMEP and related synthesis of RAFT agent (CPDB) and monomer DMMEP.

Table 1
Summary of RAFT polymerization of pHEMA and pHEMA-block-pDMMEP in DMF.

Sample	[M]:[CTA]:[I]	Conv. [%]	$M_{n,theo}$ [g mol^{-1}]	$M_{n,NMR}$ [g mol^{-1}]	$M_{n,GPC}$ [g mol^{-1}]	PDI
pHEMA	307:1:0.02	30	14,000	12,013	14,252	1.25
pHEMA-block-pDMMEP 28 kDA	68:1:0.33	90	28,000	27,515	28,249	1.18
pHEMA-block-pDMMEP 39 kDA	124:1:0.33	85	39,000	37,418	39,416	1.22

remained below 1.3 (Table 1). Fig. 3a illustrates linear behavior nearly until the end of the polymerization, which indicates a pseudo-first order reaction, which depicts constant concentration of free radicals during polymerization. After 450 min, the monomer is almost completely converted and literature known conversion was reached.

The block copolymerization was performed with the macro-RAFT agent pHEMA (14 kDa), AIBN, the internal standard (naphthalene) and the monomer DMMEP in DMF at 70 °C. The pDMMEP block was varied from 14 kDa to 25 kDa to ultimately obtain 28 kDa and 39 kDa pHEMA-block-pDMMEP polymers, respectively. Monomer conversion during block copolymerization can be determined using Equation 3 (see Supporting Information S6). Table 1 shows monomer conversion, molecular weight and molar mass dispersity of the pHEMA–block–pDMMEP block copolymers. The theoretical molecular weight was determined via Equation 4 (see Supporting Information S6). Both block copolymers were polymerized with conversions about 90% after 400 min. If there was no more significant change in monomer conversion, the polymerization was considered complete. Fig. 3b and 3c illustrate linear behavior until the end of the polymerization indicating a pseudo-first order reaction. Furthermore, they show well-controlled polymerization due to a linear increase of the conversion whereby molar mass dispersity remained below 1.3 (Table 1). The GPC analysis of pHEMA and both block copolymers is depicted in Fig. 3d and shows continuous increase of molecular weight.

The monomer conversion increases very slowly in the beginning, however, accelerates after 80 min. Fig. 3c shows a retardation in the polymer chain extension with longer second block during the first 100 min of dithiobenzoate-mediated RAFT polymerization in DMF. It is assumed that an induction period was observed as often stated for RAFT polymerization.[57] This period can be explained by the higher monomer concentration resulting in slow fragmentation[58] and/or intermediate radical models,[59,60] like the intermediate radical termination hypothesis (IRT), where intermediate radicals were consumed in side reactions (combination and disproportionation).[61] Table 1 depicts a summary of the homopolymerization and block copolymerizations including GPC measurements.

After successful RAFT polymerization of the block copolymers with different lengths of the DMMEP block, end group removal to entirely characterize the polymers adhesion using AFM based SMFS. In many cases, it is desirable to transform the thiocarbonylthio group to achieve a preferred functionality. Additionally, the presence of this group leads to a colored polymer. There are several ways to modify the end group of a

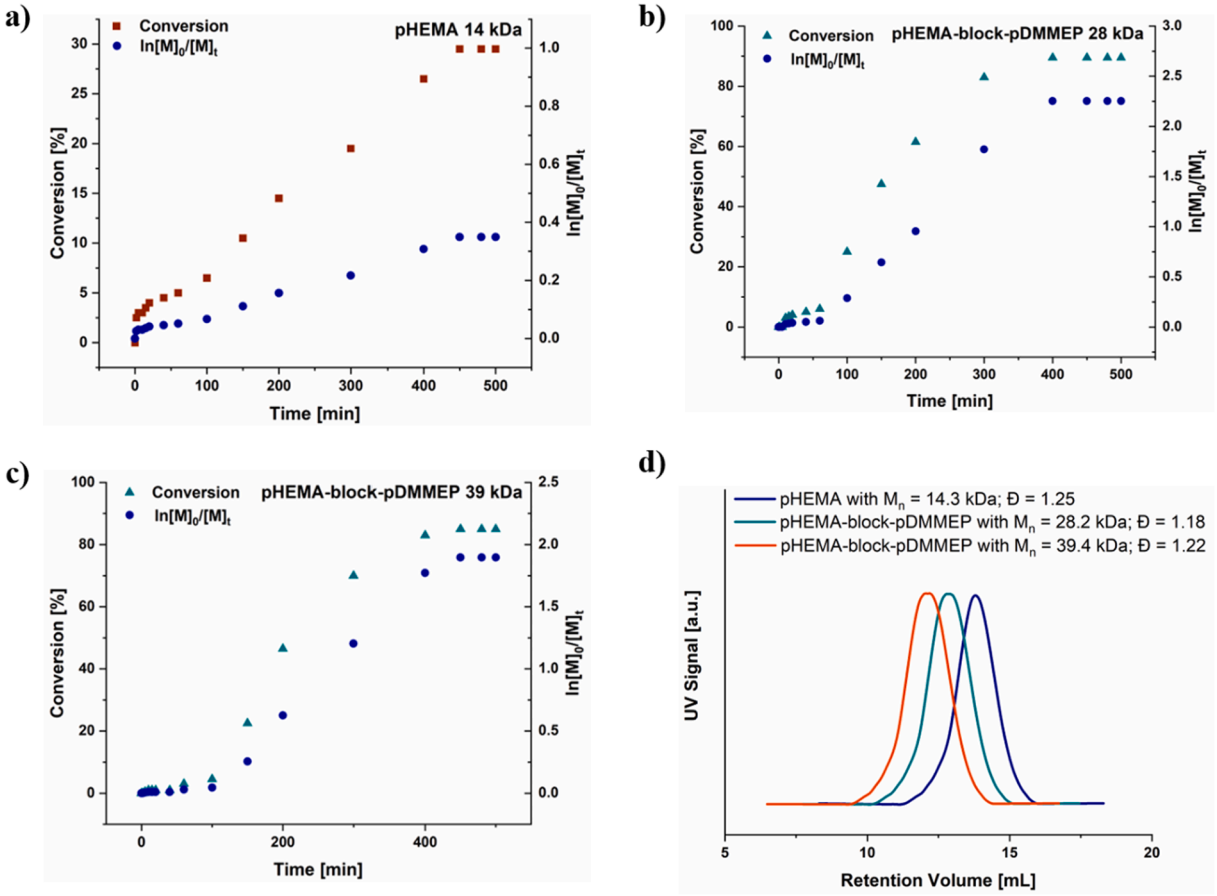

Fig. 3. a) Kinetic plot and conversion over time of RAFT polymerization of pHEMA in DMF at 70 °C with AIBN as initiator and CPDB as CTA. Kinetic plot of pHEMA-block-pDMMEP with b) 28 kDa and c) 39 kDa in DMF at 70 °C with AIBN as initiator and pHEMA as macro-CTA. d) GPC analysis of pHEMA and the block copolymers measured in DMSO at 60 °C.

RAFT polymer.[62,63] For the determination of the pull-off force via SMFS a maleimide-PEG-NHS linker is connected to the AFM tip. The free maleimide group is predestined for a Michael-type thiol-ene click reaction with a thiol group on the polymer. Therefore, an aminolysis reaction was performed to transform the thiocarbonylthio moiety into a thiol group. Disulfide formation can be reduced during the reaction with the reducing agent tris(2–carboxyethyl)phosphine (TCEP). For these reactions 0.2 eq. of the block copolymer (pHEMA-block-pDMMEP 28 kDa, 39 kDa) and 0.2 eq. of TCEP were dissolved in DMF and degassed with argon followed by addition of 1 eq. of propylamine. The polymer was precipitated in diethyl ether. NMR spectroscopy cannot be used to suggest the quantitative reduction of the dithioester end group because the signal attributed to the aromatic end group is very low. Therefore, UV–Vis spectroscopy was used as simple procedure for the characterization of the resulting polymers. The dithioester moiety has a strong absorption band at 300–310 nm in DMF. After aminolysis the absorption band of the dithioester is absent, which indicates the reduction of the dithioester terminus. Fig. 4 shows the UV–Vis absorption spectra of pHEMA-block-pDMMEP synthesized by RAFT polymerization before (solid lines) and after (dashed lines) reaction with propylamine.

GPC analysis shows no significant change in molecular weight, which indicates successful end-group removal of pHEMA-block-pDMMEP to HS-pHEMA-block-pDMMEP.

2.2. Single-molecule adhesion force of RAFT polymers

To characterize the adhesion of the 28 kDa and 39 kDa HS-pHEMA-block-pDMMEP polymers, which differ in the length of the DMMEP block, pull-off forces were measured in phosphate buffered saline (PBS) on different substrates. AFM tips were first amino-functionalized and equipped with a flexible linker to attach the two block copolymers synthesized via RAFT polymerization. The adhesion forces of these biomimetic block copolymers were investigated on calcium deficient hydroxyapatite (CDHAP) to mimic the mineral phase of the bone and tooth, on a TiO_2-coated silicon wafer to mimic implants in a physiological environment and on mica.

The functionalization of silicon nitride (Si_3N_4) AFM tips with nominal spring constants of 0.02 N m^{-1} followed an established protocol for antigen–antibody interaction measurements[64,65] modified for adhesion motifs as previously reported.[20] After oxidation of the AFM tip surface under ambient atmosphere (atmospheric oxygen), the generated silanol groups were amino-functionalized with ethanolamine. The free amino groups were then esterified with an NHS-PEG-maleimide linker with a length of about 72 nm. The free maleimide group on the linker is predestined for Michael-type maleimide-click chemistry via the free thiol group generated by the end group removal on the polymers (see Fig. 6a). The RAFT agent was selected because it does not contain any other acid groups that could interfere with the substrate during the adhesion measurement.

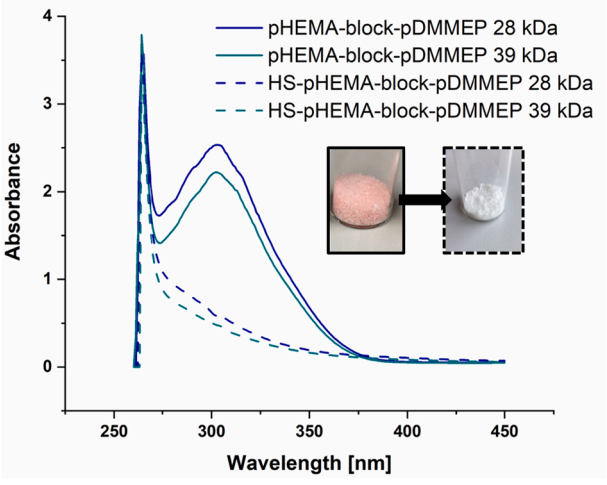

Fig. 4. UV–Vis absorption spectra of pHEMA-block-pDMMEP and HS-pHEMA-block-pDMMEP in DMF.

In a typical SMFS pull-off experiment, a functionalized AFM tip with attached adhesion motif is brought into contact with the target surface of the desired substrate (CDHAP, TiO_2 or mica) at a constant displacement rate until predefined (setpoint) force is reached. This contact was maintained over different time periods (0, 2, 4, 8 s). The functionalized AFM tip with adhesion motif is then pulled off the surface at different velocities (100–2000 nm s^{-1}), while recording force *vs* displacement data. The adhesion measurements were performed in fluid (PBS, pH 7.2). The choice of the buffer system is essential because the PEG chain changes slightly in configuration under different conditions.[66] Krysiak *et al*[67] showed that tris buffer is more suitable for SMFS adhesion measurements than others. However, we chose PBS to mimic physiological conditions on bone, considering that the hydroxyapatite surface containing calcium ions can interact with phosphate ions in PBS. As previously reported,[20] the maximum possible binding sites of a molecule per area (molecules/μm^2) at the apex of the AFM tip were determined in advance to ensure that only an individual molecule and thereby, one single adhesion motif interacts with the surface which was confirmed by the results we received. Multiple interactions and dissociation events were present in about 15% of the data as it is usually the case for this type of measurements.[68] These events were discarded for data processing.[20]

For the adhesion measurements in this study, a maleimide-PEG-NHS linker system with an average of 162 ethylene glycol units (with a calculated length of 72 nm) was used to clearly distinguish between specific and non-specific adhesions events.[20] The selected linker system generates specific adhesions events with tip-sample separation distances from 80 nm to 180 nm. Further validations for the SMFS measurements were performed as recently published.[20] Briefly, the pull-off forces were measured after each functionalization step, showing more specific adhesion events when the adhesive polymers were attached (Fig. 5). The different adhesion values after each step were also evidence for successful chemical functionalization (see Fig. 5b). Kruskal-Wallis-Test with Bonferroni post-hoc test was performed, to check significance for validation on TiO_2 (see Supporting Information S2).

The dependence of adhesion of the adhesive block copolymer pHEMA-block-pDMMEP 28 kDa on CDHAP on the surface dwell time was investigated by varying the dwell time from 0 s to 8 s and using a constant retraction velocity of 1000 nm s^{-1} (Fig. 6b). The adhesion force increased significantly with rising dwell times from 0 s to 4 s, whereas dwell times above 4 s did exhibit similar adhesion force values (Fig. 6c). Each bar in the chart presented in Fig. 6c consists of 600 measurements from four cantilevers. These results clearly show that sufficient dwell time is important for adhesion motifs to orient and arrange themselves properly on the surface. They are in perfect agreement with previous measurements in our previous published study[20] and in Krysiak *et al.*[67] Kruskal-Wallis-Test with Bonferroni post-hoc test was performed to check significance between the 28 kDa polymer by variation of dwell times on CDHAP (see Supporting Information S3). Notably, the adhesion force at dwell times of 4 s and above was 1.610 ± 0.076 nN, which is higher compared to the single-molecule adhesion force of DOPA on a Ti-substrate as reported by Lee *et al.*[69] and higher than the adhesion force of DpSpSEEKC on CDHAP and TiO_2 as reported in our own recent previous study.[20]

The mechanism of the dwell-time phenomenon remains unclear and has not been fully elucidated so far, perhaps higher dwell time is related for achieving the optimal conformation for interface formation [70] due to interfering phosphate ions from the PBS buffer.

Adhesion Force is dependent on length of phosphorus block. Two different block copolymers were synthesized by RAFT polymerization, the first block is based on the monomer HEMA with a molecular

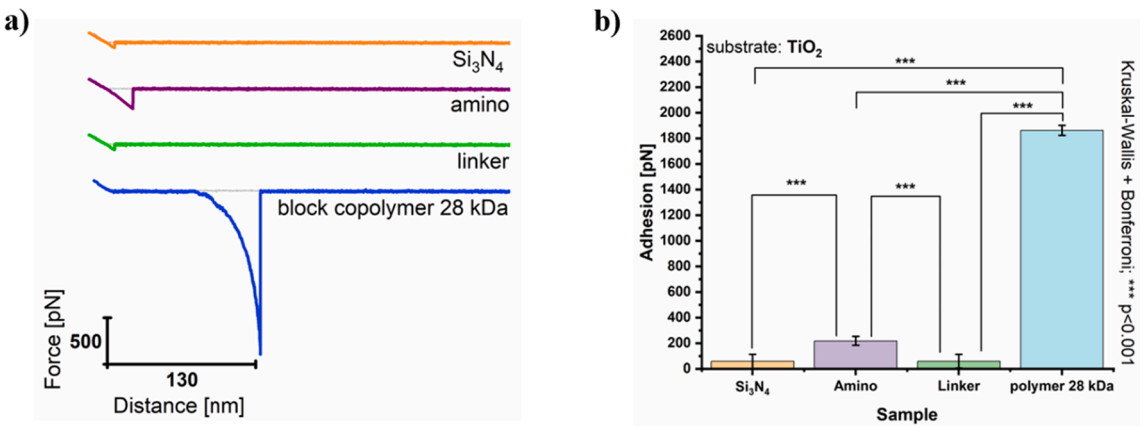

Fig. 5. Validation of SMFS measurement by comparing the pull-off forces of an unfunctionalized silicon nitride (Si_3N_4) tip, an amino functionalized tip, a linker functionalized tip and a linker-pHEMA-block-pDMMEP 28 kDa functionalized tip on TiO_2 at 4 s delay time and a retraction velocity of 1000 nm s^{-1}. a) Force/distance curves on TiO_2. b) Bars showing adhesion and statistical analysis after every functionalization step.

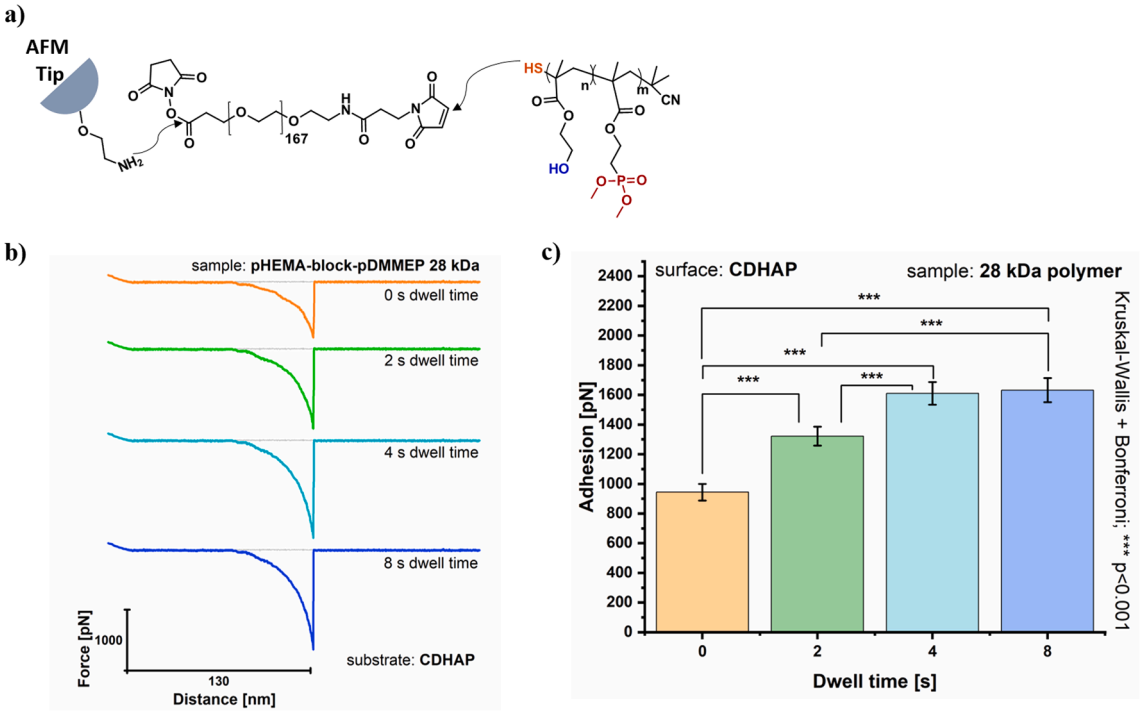

Fig. 6. a) Functionalization of AFM tip including amino- and linker-functionalization as well as introduction of the adhesive polymers. b) Selected force-distance curves of SMFS measurement with pHEMA-block-pDMMEP 28 kDa on CDHAP with different dwell times and constant retraction velocity of 1000 nm s^{-1}. c) Mean adhesion values of different dwell times, error bars indicate standard deviations.

weight of 14 kDa and the second block is composed of the monomer DMMEP, which was varied from 14 kDa to 25 kDa. These two polymers differ only in the length of the phosphonic acid containing block. Both polymers have been investigated for their adhesion strength to CDHAP, TiO_2 and mica in wet environment. In particular, the influence of the longer phosphonic acid block compared to the shorter one will be determined.

Fig. 7a shows the selected retraction force/distance (FD) curves on CDHAP for both polymers with 4 s dwell time and 1000 nm s^{-1} pull-off velocity. 600 FD curves per pulling velocity and dwell time were recorded on four spots on the substrate. Curves with distinct dissociation events from detected adhesion forces were plotted as histograms (Fig. 7b). The resulting adhesion forces are not normally distributed (Kolmogorov-Smirnov test see Supporting Information S4) and illustrate significantly higher pull-off forces (Mann-Whitney-U-Test see Supporting Information S4) of pHEMA-block-pDMMEP 39 kDa compared to ones of the 28 kDa polymer with shorter phosphonate block (Fig. 7c).

Analogous to CDHAP, the adhesion of the block copolymers to TiO_2 was evaluated. Titanium and its oxides are often used for implants. Fig. 8a depicts the comparison of FD curves of pHEMA-block-pDMMEP 28 kDa and 39 kDa on TiO_2 coated silicon wafer with 4 s dwell time and 1000 nm s^{-1} pull-off velocity. Histograms of the 28 kDa and 39 kDa polymers were plotted in Fig. 8b. The resulting adhesion forces are not normally distributed (Kolmogorov-Smirnov test see Supporting Information S5) and illustrate significantly higher pull-off forces (Mann-Whitney-U-Test see Supporting Information S5) of the polymer with longer phosphorus ester block when comparing it to the 28 kDa polymer. Fig. 8c shows again the synthesized block copolymers and demonstrates the higher adhesive force using longer phosphorus ester blocks.

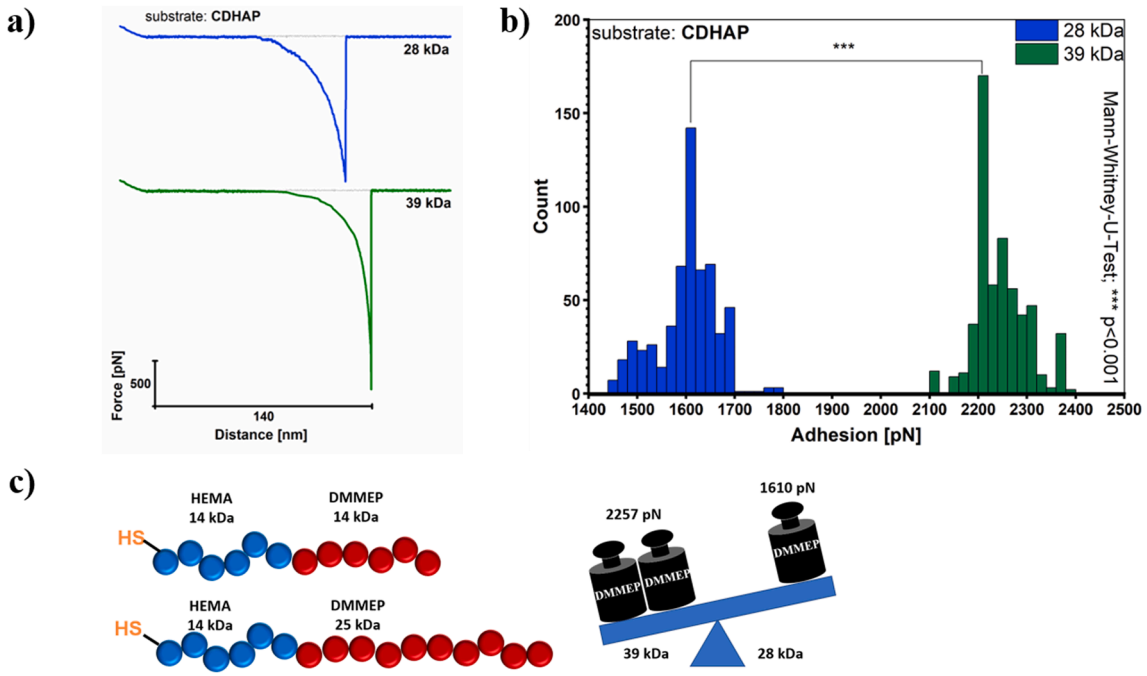

Fig. 7. SMFS measurement of pHEMA-block-pDMMEP with 28 kDa and 39 kDa on CDHAP with 4 s dwell time and a retraction velocity of 1000 nm s^{-1}. a) Selected FD curves of pHEMA-block-pDMMEP 28 kDa and 39 kDa. b) Histograms (n = 600) of adhesion forces of 28 kDa polymer (1610 ± 76 pN) and of 39 kDA polymer (2257 ± 48 pN) ($p < 0.001$) measured with four AFM tips. c) Higher phosphorylation of the polymer leads to higher adhesion on CDHAP.

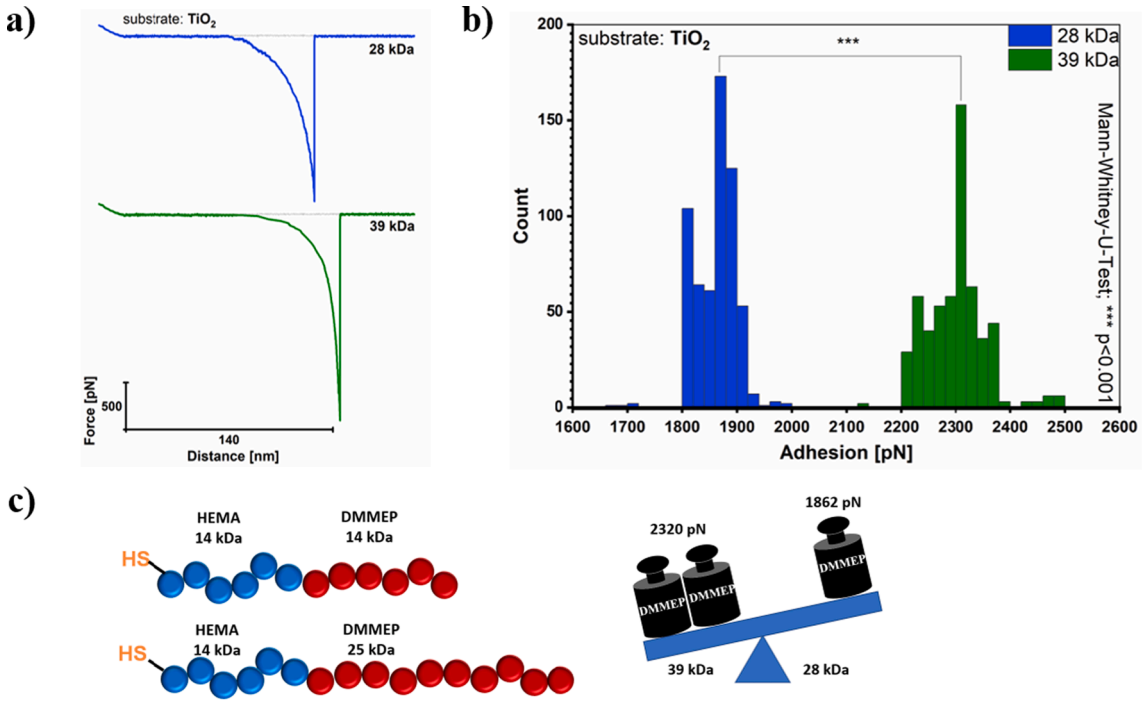

Fig. 8. SMFS measurement of pHEMA-block-pDMMEP with 28 kDa and 39 kDa on TiO_2 coated silicon wafer with 4 s dwell time and a retraction velocity of 1000 nm s^{-1}. a) Selected FD curves of pHEMA-block-pDMMEP 28 kDa and 39 kDa. b) Histograms (n = 600) of adhesion forces of 28 kDa polymer (1862 ± 39 pN) and of 39 kDA polymer (2320 ± 42 pN) ($p < 0.001$) measured with four AFM tips. c) Higher phosphorylation of the polymer leads to higher adhesion on TiO_2.

The longer block of adhesive groups increases the probability of interaction with Ti^{4+} ions and oxides of the titanium substrate as well as interaction with Ca^{2+} ions, hydroxyl groups and phosphonates of the HAP substrate. Further adhesion measurements of biomimetic RAFT polymers and statistical analysis thereof were performed on mica (see Supporting Information S1). SMFS measurements on CDHAP, TiO_2 and mica showed a distinct increase in adhesion of the polymer with longer phosphonic acid ester block. An increase in block length of 40% results in an increase in adhesion of about 25%.

We are aware that our method may has two main limitations. The first is that the occurrence of steric hindrances is related to the length of the block copolymer. In other words, block copolymers containing

longer phosphonate blocks possess higher probability to hinder binding between adhesion motif and surface groups. The scecond is the possible emergence of high adhesion forces during the SMFS experiments. Measured adhesion force values are close to rupture forces of maleimide-thiol adduct bonds[71] and other related covalent bonds.[72]

3. Conclusion

In nature and in the human body adhesive interactions of proteins are of crucial importance for a multitude of biological processes in various conditions. To maintain their adhesion capacity on surfaces in wet environments is a significant characteristic of biological adhesives.

Many synthetic adhesives proposed for industrial applications, especially in the field of tissue engineering are lacking the ability to bind to moist surfaces.

In this study, we used SMFS to show the dependence of adhesion on the length of phosphonate blocks in biomimetic block copolymers on different substrates (CDHAP, TiO_2 and mica) under physiological conditions (PBS, pH 7.2). The use of SMFS allowed use to investigate adhesion processes on the nanoscopic level and circumventing the challenge to distinguish between cohesive and adhesive forces – a common problem on the macroscale.

The synthesized polymers as well as the polymerization technique allowed us to quickly investigate and compare the adhesion of the blocks via SMFS by tethering them on the AFM tip. By using RAFT polymers, the RAFT agent end group (thiocarbonylthio group) can be removed via aminolysis and a thiol end group is generated. Thus, synthesized RAFT polymers can be attached to the functionalized AFM tip via a free maleimide group. The results of this study indicate the dependence of adhesion to the length of phosphonate blocks on three substrates, especially CDHAP to replicate the mineral part of the bone and TiO_2 to mimic implants. With the carefully selected neutral first block (HEMA), the free hydroxy group enables the introduction of a desired functional group for further applications. Although there are limitations due to the length of phosphonate blocks and the emergence of high adhesion forces during SMFS experiments, we believe our work highlights the use of adhesion motif containing block polymers. This approach may be very promising in the biomedical field, especially for tissue engineering applications.

4. Experimental

4.1. Materials

All reagents, if not otherwise mentioned, were purchased from Sigma Aldrich and were used without further purification. 2,2′-Azobisisobutyronitrile (AIBN) initiator was purified by recrystallization from methanol. 2-Hydroxyethyl methacrylate (HEMA) was distilled before polymerization. Solvents were purchased and distilled prior usage. ^{1}H-, ^{13}C- and ^{31}P NMR spectra were recorded on a Bruker Avance 400 MHz FT-NMR spectrometer. Deuterated DMSO and chloroform were used as NMR solvents.

4.2. Monomer synthesis of dimethyl (2-methycryloyloxyethylphosphonate) (DMMEP)

The synthesis of dimethyl (2-methycryloyloxyethylphosphonate) (DMMEP) was carried out according to Avci *et al.*[52] Therefore, 1 eq. of dimethyl (2-hydroxyethyl) phosphonate (15.4 g, 100 mmol) was reacted with 1.05 eq. of methacryloyl chloride (11.0 g, 105 mmol) in the presence of 1.25 eq. of triethylamine (12.7 g, 125 mmol) in 20 mL dry methylene chloride at 0 °C under Schotten-Baumann conditions. After stirring overnight at room temperature, the formed precipitate was filtered off and washed with 40 mL diethyl ether. The organic phases were combined and washed with 80 mL of brine. The pH value was adjusted to 1 with 2 N hydrochloric acid. In addition to that, the organic phases were washed with 80 mL of 10 wt% aqueous solution of $NaHCO_3$ and 100 mL of brine. Excess of triethylamine and triethylamine/HCl salts were then removed by extraction with deionized water (3 × 20 mL). The organic layer was separated and dried over $CaCl_2$. The evaporation of methylene chloride gave 18.52 g (83% of theory) of the desired product as a yellow, viscous liquid.

TLC (EE): R_f 0.20; **^{1}H NMR**: (400 MHz, $CDCl_3$) δ (ppm): 6.12 (s, 1H, CH_2 = C cis), 5.58 (s, 1H, CH_2 = C trans), 4.39 (dtd, 2H, J_1 = 13.4 Hz, J_2 = 7.3 Hz, J_3 = 1.2 Hz, O-CH_2), 3.76 (s, 6H, 2x O-CH_3), 2.19–2.07 (dtd, 2H, J_1 = 18.8 Hz, J_2 = 7.3 Hz, J_3 = 1.1 Hz, CH_2-P), 1.93 (s, 3H, CH_3); **^{13}C NMR**: (100 MHz, $CDCl_3$) δ (ppm): 167.06 (C = O), 135.97 (C = CH_2), 126.08 (C = CH_2), 58.68 (2x O-CH_3), 52.69 (O-CH_2), 25.66 (CH_2-P), 18.22 (CH_3); **^{31}P NMR**: ($CDCl_3$) δ (ppm): 29.69 (s); **GC–MS** (*m/z*): calc. 222.18, found 222.12 [M]

4.3. RAFT agent synthesis

4.3.1. Synthesis of sodium dithiobenzoate (DTBA)

The synthesis was carried out according to Mitsukami *et al.*[53] and Thang *et al.*[55] Therefore, a 500 mL three-neck round-bottomed flask equipped with a magnetic stir bar, dropping funnel and thermometer was dried, filled with argon, charged with 2 eq. of sodium methoxide (30 wt% solution in methanol; 90.38 g, 500 mmol) and diluted in 160 mL dry methanol. Subsequently, 2 eq. of sulfur (16.03 g, 500 mmol) were added under argon counter flow. 1 eq. of benzyl chloride (31.65 g, 250 mmol) was added dropwise over the course of approximately 1.5 h at room temperature. The reaction mixture was heated in an oil bath at 75 °C for 20 h. After this time, the reaction mixture was cooled to 0 °C using an ice bath. The precipitated salts were removed by filtration, washed with 50 mL of methanol and then the solvent was evaporated. The residue was dissolved in 250 mL of deionized water and the precipitated salts were removed by filtration. Hereafter, the solution was transferred into a 1 L separatory funnel and washed with diethyl ether (3 × 150 mL). Diethyl ether (150 mL) and 250 mL 1 N HCl were added to the deep red solution. Then dithiobenzoic acid was extracted into the ethereal layer (purple color). Afterwards 150 mL deionized water and 300 mL 1 N NaOH were added to the ethereal layer, whereby sodium dithiobenzoate was extracted to the orange-red aqueous layer. This washing process was repeated two more times to finally yield a 500 mL solution of sodium dithiobenzoate.

4.3.2. Synthesis of di(thiobenzoyl) disulfide (DTBDS)

For the synthesis of di(thiobenzoyl)disulfide the aqueous sodium dithiobenzoate solution was transferred to an 1 L round-bottomed flask with magnetic stirrer. Potassium ferricyanide (III) (90.38 g, 150 mmol) was dissolved in 300 mL deionized water and was added dropwise over the course of approximately 2.5 h under vigorous stirring. The red precipitate was filtered and washed with deionized water until the washings became colorless. The red solid was dried in vacuum for 6 h at room temperature to yield 16.53 g (22% theoretical yield).

TLC (PE:EE 20:1): R_f 0.67; **mp** 95–97 °C (Lit[73]: 96–98 °C); **^{1}H NMR**: (400 MHz, $CDCl_3$) δ (ppm): 7.96 (d, 4H, o-ArH), 7.63 (m, 2H, p-ArH), 7.51 (m, 4H, m-ArH); **^{13}C NMR**: (100 MHz, $CDCl_3$) δ (ppm): 167.77 (-C = S), 133.33 (-ArC-C = S), 131.21 (p-ArC), 129.73 (m-ArC), 129.04 (o-ArC); **IR** (ATR) ν (cm^{-1}): 1236.2 (C = S), 1041 (C = S)

4.3.3. Synthesis of 2-cyanopropyl-2-dithiobenzoate (CPDB)

The synthesis was performed according to Mitsukami *et al.*[53] Therefore, ethyl acetate was pre-dried over K_2CO_3 for 12 h, decanted and distilled from 10 g/L P_2O_5. A 250 mL round-bottomed flask was purged three times with argon and charged with 0.6 eq. of di(thiobenzyol)disulfide (4.69 g, 15 mmol), AIBN (1 eq., 1.73 g, 9 mmol) and dry ethyl acetate. The reaction solution was heated at reflux for 20 h. Afterwards the ethyl acetate was removed in vacuum. The crude product was purified by column chromatography (PE:EE 20:1) to yield 2.43 g (52% theoretical yield) of a red viscous liquid.

TLC (PE:EE 10:1): R_f 0.51; **^{1}H NMR**: (400 MHz, $CDCl_3$) δ (ppm): 7.91 (m, 2H, o-ArH), 7.55 (m, 1H, p-ArH), 7.39 (m, 2H, m-ArH), 1.94 (s, 3H, CH_3); **^{13}C NMR**: (100 MHz, $CDCl_3$) δ (ppm): 223.15 (-C = S), 144.59 (-ArC-C = S), 132.91 (p-ArC), 128.56 (m-ArC), 126.67 (o-ArC), 119.98 (–CN), 41.75 (-C-CN), 26.50 (2x $–CH_3$); **MS** (*m/z*): calcd. 222.34, found 221 [M]; **IR** (ATR) ν (cm^{-1}): 2232.7 (CN), 1227.3 (C = S), 1047.7 (C = S)

4.4. RAFT polymerization of adhesive block copolymers followed by end-group removal

The RAFT polymerization of pHEMA was carried out similar to Vega-Rios *et al.*[56] To perform RAFT polymerization of HEMA (14 kDa), the monomer, initiator (AIBN), RAFT-agent (CPDB) and the internal standard (naphthalene) were dissolved in DMF (M:CTA:I 230:1:0.02). The solution was degassed for about 40 min. Afterwards the penicillin flasks were placed in a pre-heated metal heating block (70 °C). The polymerization kinetics were investigated by drawing samples over the whole course of reaction. Therefore, an amount of about 200 µL of samples were taken by syringe after certain time intervals and quenched by ice cooling to stop the reaction until they were analyzed by ^{1}H NMR spectroscopy. After complete polymerization time, the reaction mixture was quenched by liquid nitrogen and precipitated in cold diethyl ether. The sticky polymer was re-dissolved in methanol and precipitated in cold diethyl ether for three more times to yield a pink powdery polymer.

^{1}H NMR: (400 MHz, DMSO-d_6) δ (ppm): 4.92–4.67 (br, 1H, –OH), 3.90 (s, 2H, -O-CH_2-), 3.60 (s, 2H, –CH_2-OH), 2.02–1.68 (br, 2H, –CH_2-), 0.95 (s, 3H, –CH_3)

The block copolymerization was done in accordance to Canniccioni *et al.*[36] The synthesis of pHEMA-block-pDMMEP (28 kDa and 39 kDa) polymers was performed via RAFT polymerization, the monomer DMMEP, AIBN, macro RAFT-agent (pHEMA) and the internal standard naphthalene were dissolved in DMF (M:CTA:I 68:1:0.33; 124:1:0.33). The solution was degassed for about 40 min. Afterwards the penicillin flaks were placed in a pre-heated metal heating block (70 °C). The polymerization kinetics were investigated by drawing samples over the whole course of reaction. Therefore, an amount of about 200 µL of samples were taken by syringe in noted time intervals and quenched by ice cooling to stop the reaction until they were analyzed by ^{1}H nuclear magnetic resonance spectroscopy (NMR). After complete polymerization time the reaction mixture was quenched by liquid nitrogen and precipitated in cold hexane. The sticky polymer was re-dissolved in methanol and precipitated in cold hexane for three more times to yield a pink polymer.

^{1}H NMR: (400 MHz, DMSO-d_6) δ (ppm): 4.97–4.62 (br, 1H, –OH), 4.17–3.91 (m, 4H, -O-CH_2–), 3.94 (s, 2H, -O-CH_2–), 3.71–3.58 (m, 8H, –CH_2-OH, 2x -O-CH_3), 2.29–1.58 (br, 4H, –CH_2–), 1.13–1.06 (br, 2H, –CH_2-P), 1.13–0.75 (br, 6H, –CH_3); **^{31}P NMR**: (DMSO-d_6) δ (ppm): 29.51 (s)

To remove the end-group of the block copolymers, 0.01 eq. of pHEMA-block-pDMMEP (28 kDa, 39 kDa) and TCEP (0.01 eq.) were dissolved in DMF. Afterwards the solution was degassed and 0.05 eq. of propylamine were added. The solution was stirred for about 2 h and the product was precipitated in cold diethyl ether. The sticky polymer was re-dissolved in methanol and precipitated again in cold diethyl ether for three more times to yield a colorless polymer.

^{1}H NMR: (400 MHz, DMSO-d_6) δ (ppm): 4.97–4.62 (br, 1H, –OH), 4.17–3.91 (m, 4H, -O-CH_2–), 3.94 (s, 2H, -O-CH_2–), 3.71–3.58 (m, 8H, –CH_2-OH, 2x -O-CH_3), 2.29–1.58 (br, 4H, –CH_2–), 1.13–1.06 (br, 2H, –CH_2-P), 1.13–0.75 (br, 6H, –CH_3); **^{31}P NMR**: (DMSO–d_6) δ (ppm): 29.51 (s)

4.5. Polymer characterization via gel permeation chromatography (GPC)

Molecular weight of the polymers was determined by gel permeation chromatography (GPC) measurements using a Viscotek® GPCmax VE2001 system with a UV detector (Viscotek® detector) and three columns (AplliChrom DMSO-Phil-P-200, AplliChrom DMSO-Phil-P-250, DMSO-Phil-P-350) (AplliChrom, Oranienburg, Germany) with dry DMSO as mobile phase (0.5 mL min^{-1} flow rate) at 60 °C. The polymers were dissolved in dry DMSO, filtered through a 0.2 µm poly(tetrafluoroethylene) (PTFE) disposable Chromafil 0–20/15MS syringe filter. The injection volume was 100 µL. Calibration was performed with polymethylmethacrylate standards (Agilent Technologies, M_n range between 550 and 46890 g mol^{-1}). Omnisec Software was used for determination of M_n and M_w to calculate the molar mass dispersity (Đ).

4.6. AFM tip functionalization

AFM tips for force spectroscopy measurements were prepared according to previous published functionalization protocol.[20] Prior to functionalization silicon nitride (Si_3N_4) AFM chips (Bruker MSNL-10) were oxidized in ambient atmosphere (atmospheric oxygen) and cleaned in chloroform (3 × 5 min). The AFM tips with silanol (Si-OH) groups were dried in a gentle argon stream. Subsequently, the tips were immersed in 1 g mL^{-1} ethanolamine hydrochloride (TCI Deutschland, Eschborn, Germany) dissolved in DMSO in the presence of molecular sieves (4 Å) for 30 min, resulting in an amino-functionalized AFM tip. The aminated AFM tips were washed with DMSO (3 × 1 min) and ethanol (3 × 1 min) and dried in a gentle argon stream. Maleimidopropionyl-PEG-hydroxysuccinimide ester (Mal-PEG-NHS with an average of 162 ethylene glycol units, JenKem Technology, USA) were used as linker and covalently coupled to the amino-functionalized tips in a Teflon reaction chamber by incubating cantilevers with a solution of 7 mg Mal-PEG-NHS linker dissolved in 1 mL of chloroform. 150 µL of triethylamine were added to the linker solution. After 2 h of reaction time the AFM tips were washed with chloroform (3 × 10 min) and dried in a gentle argon stream. For attachment of the synthesized copolymers to the linker system, the sample was dissolved in 100 µL deionized water to obtain a 15 mM solution. This solution was mixed with ethylenediamine tetraacetic acid (EDTA), 4-(2-hydroxyethyl)-1-piperazineethanesulfonic acid (HEPES) and tris(2-carboxyethyl) phosphine (TCEP; TCI Deutschland, Eschborn, Germany). Subsequently, 100 µL of this solution were pipetted onto the AFM chips, which were placed on pieces of Parafilm in Petri dishes. After 2 h reaction time the tips were washed (3 × 5 min) and stored at 4 °C for up to two days in PBS buffer (pH 7.2 – 7.4; sterile filtered).

4.7. Substrate preparation

The preparation and characterization of the calcium deficient hydroxyapatite (CDHAP) pellet was the same as previously published.[20] The silicon wafer [Si-Mat, Kaufering,Germany; crystal structure of (1 0 0)] was cleaned by a UV cleaner (Boekel Scientific, Pennsylvania, USA) for 15 min prior usage. Afterwards, it was sonicated in water, methanol, acetone and toluene followed by coating of TiO_2 nanoparticles. The layer thickness of the TiO_2-layered wafer was determined by ellipsometry (Sentech SE 500adv, Sentech Instruments, Berlin, Germany). The same TiO_2 coated silicon wafer was used and characterized in Steinbauer *et al.*[20]

4.8. AFM-SMFS measurements

All AFM experiments were performed in PBS buffer with high quality chemicals in a temperature- and humidity-controlled room at a temperature of 20.7 ± 0.7 °C and humidity of 47.9 ± 6.7%. The measurements were conducted on a NanoWizard ultra speed atomic force microscope (JPK Instruments, Berlin, Germany) using Bruker MSNL-10 cantilevers (<12 nm tip radius, 0.02 N m^{-1} nominal spring constant) in liquid under physiological-like conditions (PBS, pH 7.2) on different substrates (mica, CDHAP, TiO_2 coated Si-wafer). The AFM was operated with an inverted optical microscope Axio Observer, AxioVert 200 (Zeiss,

Germany). The NanoWizard is placed on a Halcyonics i4 vibration isolation system (Accurion, Göttingen, Germany) and the whole system is located in an acoustic enclosure from JPK, which in turn is placed on a stable base (JPK, Berlin, Germany). Prior functionalization AFM tips were cleaned in chloroform and cantilever spring constants were determined under dry conditions using thermal method (Sader method). [74] Nominal spring constants (k_c) between 7.7 and 9.8 mN m^{-1} were obtained. After AFM tip functionalization cantilever sensitivity was measured in PBS buffer. The Inverse Optical Lever Sensitivity (InvOLS) was defined by performing sixteen force curves on a stiff substrate (mica). A linear fit was performed to each force curve.

4.9. Data analysis

Data acquisition and analysis were carried out using SPM Control and JPK data processing software. Prior to analysis, only single rupture events (adhesion events) with the specific linker stretching and ± 20 nm of the calculated contour length were taken into account ensuring over 95% probability to be sure that the adhesion event was mediated by a single bound. Due to this restriction of data, some of the curves are eliminated, but the others provide a narrow distribution of the pull off forces.

4.10. Statistical analysis

The statistical Analysis was performed with the statistic software IBM statistics SPSS. The samples were independent and the grouping variable were the tip sample and the dwell time. To test the significance of the adhesion values of the samples measured on mica, on CDHAP and on a TiO2 coated silicon wafer, all samples with a dwell time of 4 s were chosen. Before testing the significance of the mean values of adhesion, the normality of the data distribution was tested. Kruskal-Wallis-Tests with Bonferroni post-hoc tests were performed, to check significance between the sample by variation of dwell times on CDHAP (Supporting Information S3) and the validation on TiO_2 (Supporting Information S2). Due to the fact that, the mean value of several not normally distributed samples has to be compared, a Mann-Whitney-U-Test was done.

CRediT authorship contribution statement

Patrick Steinbauer: Validation, Formal analysis, Investigation, Writing - original draft, Visualization. **Andreas Rohatschek:** Validation, Data curation, Writing - review & editing. **Orestis Andriotis:** Validation, Data curation, Writing - review & editing, Supervision. **Nikolaos Bouropoulos:** Writing - review & editing. **Robert Liska:** Conceptualization, Writing - review & editing, Supervision. **Philipp J. Thurner:** Writing - review & editing, Supervision. **Stefan Baudis:** Conceptualization, Writing - review & editing, Supervision, Project administration, Funding acquisition.

Declaration of Competing Interest

The authors declare that they have no known competing financial interests or personal relationships that could have appeared to influence the work reported in this paper.

Acknowledgements

Funding by the Christian Doppler Research Association (Christian Doppler Laboratory for Advanced Polymers for biomaterials and 3D Printing), the Austrian Federal Ministry for Digital and Economic Affairs, the National Foundation for Research, Technology and Development, and the TU Wien Biointerface doctorate school are gratefully acknowledged. A.R. is a recipient of a DOC Fellowship of the Austrian Academy of Sciences at the Institute of Lightweight Design and Structural Biomechanics at TU Wien.

Data availability

The raw/processed data required to reproduce these findings cannot be shared at this time as the data also forms part of an ongoing study.

Appendix A. Supplementary data

Supplementary data to this article can be found online at https://doi.org/10.1016/j.eurpolymj.2020.110188.

References

[1] J. von Byern, I. Grunwald, Biological Adhesive Systems : from nature to technical and medical application, SPRINGER Verlag GMBH, 2016.
[2] P. Kord Forooshani, B.P. Lee, Recent approaches in designing bioadhesive materials inspired by mussel adhesive protein, J. Polym. Sci. Part A Polym. Chem. 55 (2017) 9–33, https://doi.org/10.1002/pola.28368.
[3] J.H. Waite, Mussel adhesion – essential footwork, J. Exp. Biol. 220 (2017) 517. http://jeb.biologists.org/content/220/4/517.abstract.
[4] H. Zhao, C. Sun, R.J. Stewart, J.H. Waite, Cement proteins of the tube-building polychaete <i>Phragmatopoma californica<i>, J. Biol. Chem. 280 (2005) 42938–42944, https://doi.org/10.1074/jbc.M508457200.
[5] H. Shao, J. Stewart Russell, Biomimetic Underwater Adhesives with Environmentally Triggered Setting Mechanisms, Adv. Mater. 22 (2009) 729–733, https://doi.org/10.1002/adma.200902380.
[6] C.S. Wang, N.N. Ashton, R.B. Weiss, R.J. Stewart, Peroxinectin catalyzed dityrosine crosslinking in the adhesive underwater silk of a casemaker caddisfly larvae, Hysperophylax occidentalis, Insect Biochem. Mol. Biol. 54 (2014) 69–79, https://doi.org/10.1016/j.ibmb.2014.08.009.
[7] Y. Wang, K. Sanai, M. Nakagaki, A novel bioadhesive protein of silk filaments spun underwater by caddisfly larvae, in: Adv. Mater. Res., Trans Tech Publications Ltd, 2009: pp. 1631–1634. https://doi.org/10.4028/www.scientific.net/AMR.79-82.1631.
[8] R.J. Stewart, C.S. Wang, Adaptation of caddisfly larval silks to aquatic habitats by phosphorylation of h-fibroin serines, Biomacromolecules 11 (2010) 969–974, https://doi.org/10.1021/bm901426d.
[9] E. Hennebert, Adhesion Mechanisms Developed by Sea Stars: A Review of the Ultrastructure and Composition of Tube Feet and Their Secretion, in, Biol. Adhes. Syst., Springer Vienna (2010) 99–109, https://doi.org/10.1007/978-3-7091-0286-2_7.
[10] N. Blom, S. Gammeltoft, S. Brunak, Sequence and structure-based prediction of eukaryotic protein phosphorylation sites, J. Mol. Biol. 294 (1999) 1351–1362, https://doi.org/10.1006/jmbi.1999.3310.
[11] C.L. Duvall, W.R. Taylor, D. Weiss, A.M. Wojtowicz, R.E. Guldberg, Impaired Angiogenesis, Early Callus Formation, and Late Stage Remodeling in Fracture Healing of Osteopontin-Deficient Mice, J. Bone Miner. Res. 22 (2006) 286–297, https://doi.org/10.1359/jbmr.061103.
[12] A.A. Poundarik, T. Diab, G.E. Sroga, A. Ural, A.L. Boskey, C.M. Gundberg, D. Vashishth, Dilatational band formation in bone, Proc. Natl. Acad. Sci. 109 (2012) 19178–19183, https://doi.org/10.1073/PNAS.1201513109.
[13] P.J. Thurner, C.G. Chen, S. Ionova-Martin, L. Sun, A. Harman, A. Porter, J.W. Ager, R.O. Ritchie, T. Alliston, Osteopontin deficiency increases bone fragility but preserves bone mass, Bone 46 (2010) 1564–1573, https://doi.org/10.1016/j.bone.2010.02.014.
[14] E.M. Lewiecki, Bisphosphonates for the treatment of osteoporosis: insights for clinicians, Ther. Adv. Chronic Dis. 1 (2010) 115–128.
[15] G.H. Nancollas, R. Tang, R.J. Phipps, Z. Henneman, S. Gulde, W. Wu, A. Mangood, R.G.G. Russell, F.H. Ebetino, Novel insights into actions of bisphosphonates on bone: differences in interactions with hydroxyapatite, Bone 38 (2006) 617–627.
[16] Y. Cui, T. Zhu, D. Li, Z. Li, Y. Leng, X. Ji, H. Liu, D. Wu, J. Ding, Bisphosphonate-Functionalized Scaffolds for Enhanced Bone Regeneration, Adv. Healthc. Mater. 8 (2019) 1–21, https://doi.org/10.1002/adhm.201901073.
[17] K. Shimoda, T. Mitsuoka, K. Ueda, H. Suemune, G. Hirai, M. Aso, Synthesis of dendritic bisphosphonates as bone targeting ligands, Tetrahedron Lett. 59 (2018) 4528–4531.
[18] D. Heymann, B. Ory, F. Gouin, J.R. Green, F. Rédini, Bisphosphonates: New therapeutic agents for the treatment of bone tumors, Trends Mol. Med. 10 (2004) 337–343, https://doi.org/10.1016/j.molmed.2004.05.007.
[19] J.R. Long, W.J. Shaw, P.S. Stayton, G.P. Drobny, Structure and Dynamics of Hydrated Statherin on Hydroxyapatite As Determined by Solid-State NMR, Biochemistry 40 (2001) 15451–15455, https://doi.org/10.1021/bi010864c.
[20] P. Steinbauer, A. Rohatschek, O. Andriotis, N. Bouropoulos, R. Liska, P.J. Thurner, S. Baudis, Single-Molecule Force Spectroscopy Reveals Adhesion-by-Demand in Statherin at the Protein-Hydroxyapatite Interface, Langmuir 36 (2020) 13292–13300, https://doi.org/10.1021/acs.langmuir.0c02325.
[21] N. Moszner, U. Salz, J. Zimmermann, Chemical aspects of self-etching enamel–dentin adhesives: A systematic review, Dent. Mater. 21 (2005) 895–910, https://doi.org/10.1016/j.dental.2005.05.001.
[22] S. Monge, B. Canniccioni, A. Graillot, J.-J. Robin, Phosphorus-Containing Polymers: A Great Opportunity for the Biomedical Field, Biomacromolecules 12 (2011) 1973–1982, https://doi.org/10.1021/bm2004803.

[23] S.-W. Huang, R.-X. Zhuo, Recent Advances in Polyphosphoester and Polyphosphoramidate-Based Biomaterials, Phosphorus, Sulfur Silicon Relat. Elem. 183 (2008) 340–348, https://doi.org/10.1080/10426500701734620.
[24] Y. Iwasaki, Bone Mineral Affinity of Polyphosphodiesters, Molecules 25 (2020) 758, https://doi.org/10.3390/molecules25030758.
[25] A. Clearfield, Coordination chemistry of phosphonic acids with special relevance to rare earths, J. Alloy. Compd. 418 (2006) 128–138, https://doi.org/10.1016/j.jallcom.2005.08.109.
[26] A. Clearfield, Recent advances in metal phosphonate chemistry, Curr. Opin. Solid State Mater. Sci. 1 (1996) 268–278, https://doi.org/10.1016/S1359-0286(96)80094-5.
[27] A. Clearfield, Recent advances in metal phosphonate chemistry II, Curr. Opin. Solid State Mater. Sci. 6 (2002) 495–506, https://doi.org/10.1016/S1359-0286(02)00151-1.
[28] T.P. Knepper, Synthetic chelating agents and compounds exhibiting complexing properties in the aquatic environment, TrAC - Trends Anal. Chem. 22 (2003) 708–724, https://doi.org/10.1016/S0165-9936(03)01008-2.
[29] C.C. Colyer, W.C. Gergel, Detergents/dispersants, in: Chem. Technol. Lubr., Springer US, 1994: pp. 62–82. https://doi.org/10.1007/978-1-4615-3554-6_3.
[30] J. Canadell, B.J. Hunt, A.G. Cook, A. Mantecón, V. Cádiz, Flame retardance and shrinkage reduction of polystyrene modified with acrylate-containing phosphorus and crosslinkable spiro-orthoester moieties, Polym. Degrad. Stab. 92 (2007) 1482–1490, https://doi.org/10.1016/j.polymdegradstab.2007.05.017.
[31] E. Matczak-Jon, V. Videnova-Adrabińska, Supramolecular chemistry and complexation abilities of diphosphonic acids, Coord. Chem. Rev. 249 (2005) 2458–2488, https://doi.org/10.1016/j.ccr.2005.06.001.
[32] S. Ananda Kumar, A. Sasikumar, Studies on novel silicone/phosphorus/sulphur containing nano-hybrid epoxy anticorrosive and antifouling coatings, Prog. Org. Coatings. 68 (2010) 189–200, https://doi.org/10.1016/j.porgcoat.2010.02.005.
[33] G. Moad, E. Rizzardo, S.H. Thang, A RAFT Tutorial, Strem Chem. XXV, No.1 (2011) 56. https://www.strem.com/resource/1/the_strem_chemiker.
[34] A.B. Lowe, C.L. McCormick, Reversible addition–fragmentation chain transfer (RAFT) radical polymerization and the synthesis of water-soluble (co) polymers under homogeneous conditions in organic and aqueous media, Prog. Polym. Sci. 32 (2007) 283–351.
[35] G. Moad, E. Rizzardo, S.H. Thang, Living radical polymerization by the RAFT process–a third update, Aust. J. Chem. 65 (2012) 985–1076.
[36] B. Canniccioni, S. Monge, G. David, J.-J. Robin, RAFT polymerization of dimethyl (methacryloyloxy)methyl phosphonate and its phosphonic acid derivative: a new opportunity for phosphorus-based materials, Polym. Chem. 4 (2013) 3676–3685, https://doi.org/10.1039/C3PY00426K.
[37] B.D. Fairbanks, P.A. Gunatillake, L. Meagher, Biomedical applications of polymers derived by reversible addition–fragmentation chain-transfer (RAFT), Adv. Drug Deliv. Rev. 91 (2015) 141–152.
[38] F. Karimi, T.G. McKenzie, A.J. O'Connor, G.G. Qiao, D.E. Heath, Nano-scale clustering of integrin-binding ligands regulates endothelial cell adhesion, migration, and endothelialization rate: Novel materials for small diameter vascular graft applications, J. Mater. Chem. B 5 (2017) 5942–5953, https://doi.org/10.1039/c7tb01298e.
[39] C.E. Brubaker, P.B. Messersmith, The present and future of biologically inspired adhesive interfaces and materials, Langmuir 28 (2012) 2200–2205, https://doi.org/10.1021/la300044v.
[40] J. Adelsberger, A. Kulkarni, A. Jain, W. Wang, A.M. Bivigou-Koumba, P. Busch, V. Pipich, O. Holderer, T. Hellweg, A. Laschewsky, P. Müller-Buschbaum, C. M. Papadakis, Thermoresponsive PS-b-PNIPAM-b-PS Micelles: Aggregation Behavior, Segmental Dynamics, and Thermal Response, Macromolecules. 43 (2010) 2490–2501, https://doi.org/10.1021/ma902714p.
[41] B. Du, A. Mei, Y. Yang, Q. Zhang, Q. Wang, J. Xu, Z. Fan, Synthesis and micelle behavior of (PNIPAm-PtBA-PNIPAm)m amphiphilic multiblock copolymer, Polymer (Guildf). 51 (2010) 3493–3502, https://doi.org/10.1016/j.polymer.2010.06.007.
[42] J. Skey, R.K. O'Reilly, Synthesis of chiral micelles and nanoparticles from amino acid based monomers using RAFT polymerization, J. Polym. Sci., Part A: Polym. Chem. 46 (2008) 3690–3702, https://doi.org/10.1002/pola.22710.
[43] J. Bernard, A. Favier, L. Zhang, A. Nilasaroya, T.P. Davis, C. Barner-Kowollik, M. H. Stenzel, Poly(vinyl ester) Star Polymers via Xanthate-Mediated Living Radical Polymerization: From Poly(vinyl alcohol) to Glycopolymer Stars, Macromolecules 38 (2005) 5475–5484, https://doi.org/10.1021/ma050050u.
[44] M. Barón, K.H. Hellwich, M. Hess, K. Horie, A.D. Jenkins, R.G. Jones, J. Kahovec, P. Kratochvíl, W.V. Metanomski, W. Mormann, R.F.T. Stepto, J. Vohlídal, E. S. Wilks, Glossary of class names of polymers based on chemical structure and molecular architecture (iupac recommendations, 2009), Pure Appl. Chem. 81 (2009) 1131–1186, https://doi.org/10.1351/PAC-REC-08-01-30.
[45] J. Li, J. Ren, Y. Cao, W. Yuan, Synthesis of biodegradable pentaarmed star-block copolymers via an asymmetric BIS-TRIS core by combination of ROP and RAFT: From star architectures to double responsive micelles, Polymer (Guildf). 51 (2010) 1301–1310, https://doi.org/10.1016/j.polymer.2010.01.037.
[46] H. Chaffey-Millar, M.H. Stenzel, T.P. Davis, M.L. Coote, C. Barner-Kowollik, Design Criteria for Star Polymer Formation Processes via Living Free Radical Polymerization, Macromolecules 39 (2006) 6406–6419, https://doi.org/10.1021/ma060964w.
[47] H. Chaffey-Millar, M. Busch, T.P. Davis, M.H. Stenzel, C. Barner-Kowollik, Advanced Computational Strategies for Modelling the Evolution of Full Molecular Weight Distributions Formed During Multiarmed (Star) Polymerisations, Macromol. Theory Simulations. 14 (2005) 143–157, https://doi.org/10.1002/mats.200400075.
[48] M. Luzon, C. Boyer, C. Peinado, T. Corrales, M. Whittaker, L. Tao, T.P. Davis, Water-soluble, thermoresponsive, hyperbranched copolymers based on PEG-methacrylates: Synthesis, characterization, and LCST behavior, J. Polym. Sci., Part A: Polym. Chem. 48 (2010) 2783–2792, https://doi.org/10.1002/pola.24027.
[49] W.-J. Wang, D. Wang, B.-G. Li, S. Zhu, Synthesis and Characterization of Hyperbranched Polyacrylamide Using Semibatch Reversible Addition−Fragmentation Chain Transfer (RAFT) Polymerization, Macromolecules 43 (2010) 4062–4069, https://doi.org/10.1021/ma100224v.
[50] Z. Ge, S. Luo, S. Liu, Syntheses and self-assembly of poly(benzyl ether)-b-poly(N-isopropylacrylamide) dendritic–linear diblock copolymers, J. Polym. Sci., Part A: Polym. Chem. 44 (2006) 1357–1371, https://doi.org/10.1002/pola.21261.
[51] Z. Ge, D. Chen, J. Zhang, J. Rao, J. Yin, D. Wang, X. Wan, W. Shi, S. Liu, Facile synthesis of dumbbell-shaped dendritic-linear-dendritic triblock copolymer via reversible addition-fragmentation chain transfer polymerization, J. Polym. Sci., Part A: Polym. Chem. 45 (2007) 1432–1445, https://doi.org/10.1002/pola.21914.
[52] D. Avci, A.Z. Albayrak, Synthesis and copolymerization of new phosphorus-containing acrylates, J. Polym. Sci., Part A: Polym. Chem. 41 (2003) 2207–2217, https://doi.org/10.1002/pola.10768.
[53] Y. Mitsukami, M.S. Donovan, A.B. Lowe, C.L. McCormick, Water-Soluble Polymers. 81. Direct Synthesis of Hydrophilic Styrenic-Based Homopolymers and Block Copolymers in Aqueous Solution via RAFT, Macromolecules 34 (2001) 2248–2256, https://doi.org/10.1021/ma0018087.
[54] F. Becke, H. Hagen, Production of aromatic dithiocarboxylic acids, (1972). https://www.google.ch/patents/US3636089.
[55] S.H. Thang, Y.K. Chong, R.T.A. Mayadunne, G. Moad, E. Rizzardo, A novel synthesis of functional dithioesters, dithiocarbamates, xanthates and trithiocarbonates, Tetrahedron Lett. 40 (1999) 2435–2438, https://doi.org/10.1016/S0040-4039(99)00177-X.
[56] A. Vega-Rios, A. Licea-Claveríe, Controlled Synthesis of Block Copolymers containing N-isopropylacrylamide by Reversible Addition-Fragmentation Chain-Transfer (RAFT) Polymerization, J. Mex. Chem. Soc. 55 (2011) 21–32.
[57] X. Zhang, O. Giani, S. Monge, J.J. Robin, RAFT polymerization of N, N-diethylacrylamide: Influence of chain transfer agent and solvent on kinetics and induction period, Polymer (Guildf). 51 (2010) 2947–2953, https://doi.org/10.1016/j.polymer.2010.04.073.
[58] A. Feldermann, M.L. Coote, M.H. Stenzel, T.P. Davis, C. Barner-Kowollik, Consistent experimental and theoretical evidence for long-lived intermediate radicals in living free radical polymerization, J. Am. Chem. Soc. 126 (2004) 15915–15923, https://doi.org/10.1021/ja046292b.
[59] M.J. Monteiro, H. De Brouwer, Intermediate radical termination as the mechanism for retardation in reversible addition-fragmentation chain transfer polymerization, Macromolecules 34 (2001) 349–352, https://doi.org/10.1021/ma001484m.
[60] D. Konkolewicz, B.S. Hawkett, A. Gray-Weale, S. Perkier, Raft polymerization kinetics: How long are the cross-terminating oligomers? J. Polym. Sci., Part A: Polym. Chem. 47 (2009) 3455–3466, https://doi.org/10.1002/pola.23385.
[61] G. Moad, Mechanism and Kinetics of Dithiobenzoate-Mediated RAFT Polymerization - Status of the Dilemma, Macromol. Chem. Phys. 215 (2014) 9–26, https://doi.org/10.1002/macp.201300562.
[62] M. Chen, G. Moad, E. Rizzardo, Thiocarbonylthio end group removal from RAFT-synthesized polymers by a radical-induced process, J. Polym. Sci., Part A: Polym. Chem. 47 (2009) 6704–6714.
[63] G. Moad, E. Rizzardo, S.H. Thang, End-functional polymers, thiocarbonylthio group removal/transformation and reversible addition–fragmentation–chain transfer (RAFT) polymerization, Polym. Int. 60 (2011) 9–25, https://doi.org/10.1002/pi.2988.
[64] M. Koehler, A. Fis, H.J. Gruber, P. Hinterdorfer, AFM-Based Force Spectroscopy Guided by Recognition Imaging: A New Mode for Mapping and Studying Interaction Sites at Low Lateral Density, Methods Protoc. 2 (2019) 6.
[65] L. Wildling, C. Rankl, T. Haselgrübler, H.J. Gruber, M. Holy, A.H. Newman, M.-F. Zou, R. Zhu, M. Freissmuth, H.H. Sitte, P. Hinterdorfer, Probing Binding Pocket of Serotonin Transporter by Single Molecular Force Spectroscopy on Living Cells, J. Biol. Chem. 287 (2012) 105–113, https://doi.org/10.1074/jbc.M111.304873.
[66] F. Oesterhelt, M. Rief, H.E. Gaub, Single molecule force spectroscopy by AFM indicates helical structure of poly (ethylene-glycol) in water, New J. Phys. 1 (1999) 6.
[67] S. Krysiak, Q. Wei, K. Rischka, A. Hartwig, R. Haag, T. Hugel, Adsorption mechanism and valency of catechol-functionalized hyperbranched polyglycerols, Beilstein J. Org. Chem. 11 (2015) 828–836, https://doi.org/10.3762/bjoc.11.92.
[68] H. Lee, S.M. Dellatore, W.M. Miller, P.B. Messersmith, Mussel-Inspired Surface Chemistry for Multifunctional Coatings, Science (80-.). 318 (2007) 426. http://science.sciencemag.org/content/318/5849/426.abstract.
[69] H. Lee, N.F. Scherer, P.B. Messersmith, Single-molecule mechanics of mussel adhesion, Proc. Natl. Acad. Sci. 103 (2006) 12999–13003. http://www.pnas.org/content/103/35/12999.abstract.
[70] A. Hartwig, R. Meissner, C. Merten, P. Schiffels, P. Wand, I. Grunwald, Mutual Influence Between Adhesion and Molecular Conformation: Molecular Geometry is a Key Issue in Interphase Formation, J. Adhes. 89 (2013) 77–95, https://doi.org/10.1080/00218464.2013.731363.
[71] W. Huang, X. Wu, X. Gao, Y. Yu, H. Lei, Z. Zhu, Y. Shi, Y. Chen, M. Qin, W. Wang, Y. Cao, Maleimide–thiol adducts stabilized through stretching, Nat. Chem. 11 (2019) 310–319, https://doi.org/10.1038/s41557-018-0209-2.

[72] M. Grandbois, M. Beyer, M. Rief, H. Clausen-Schaumann, H.E. Gaub, How Strong Is a Covalent Bond?, Science (80-.). 283 (1999) 1727. http://science.sciencemag.org/content/283/5408/1727.abstract.
[73] B. Li, D. Majonis, P. Liu, M.A. Winnik, Synthesis and characterization of a naphthalimide–dye end-labeled copolymer by reversible addition–fragmentation chain transfer (RAFT) polymerization, Can. J. Chem. 89 (2011) 317–325, https://doi.org/10.1139/V10-134.
[74] J.L. Hutter, J. Bechhoefer, Calibration of atomic-force microscope tips, Rev. Sci. Instrum. 64 (1993) 1868–1873.